Catalysis Communications 12 (2010) 231–237

Contents lists available at ScienceDirect

Catalysis Communications

journal homepage: www.elsevier.com/locate/catcom

Short Communication

Carbon-stabilized mesoporous MoS_2 — Structural and surface characterization with spectroscopic and catalytic tools

Mykola Polyakov [a,1], Martha Poisot [b,2], Maurits W.E. van den Berg [a,3], Thomas Drescher [a], Andriy Lotnyk [c], Lorenz Kienle [c], Wolfgang Bensch [b], Martin Muhler [a], Wolfgang Grünert [a,*]

[a] Laboratory of Industrial Chemistry, Ruhr University Bochum, D-44780 Bochum, Germany
[b] Institute of Inorganic Chemistry, Christian Albrechts University Kiel, Germany
[c] Faculty of Engineering, Institute for Material Science, Synthesis and Real Structure, Christian Albrechts University Kiel, Germany

ARTICLE INFO

Article history:
Received 11 June 2010
Received in revised form 31 August 2010
Accepted 3 September 2010
Available online 16 September 2010

Keywords:
Carbon-stabilized MoS_2
Texture
Active sites
Hydrogenation
H_2/D_2 exchange

ABSTRACT

Structural and surface properties of carbon-containing mesoporous MoS_2 and of a reference MoS_2 were studied with various techniques including XRD, elemental analysis, TEM, XPS, EXAFS, nitrogen physisorption, oxygen chemisorption (OCS), determination of exchangeable surface hydrogen, and kinetic study of test reactions like ethene hydrogenation and H_2/D_2 exchange. The study was made before and after use of these catalysts in the hydrodesulfurization of dibenzothiophene. The microstructure of carbon-stabilized MoS_2 is characterized by nanoslabs of ≈2 nm average stacking height embedded in an amorphous matrix with a very broad pore-size distribution. Thermal stress induced a collapse of the microporous structure leading to the formation of mainly mesopores. The carbon is well-distributed over the bulk, without any signature of carbide species detected neither in XPS nor in EXAFS measurements. The activity patterns of both materials (related to the OCS capacity) were similar despite the differing sulfur content, with the carbon-stabilized MoS_2 being more sulfur deficient. This suggests that the catalytic properties of the latter material were caused by near-stoichiometric MoS_2 apparently present in the nanoslabs, whereas the sulfur vacancies in the sulfur-deficient amorphous phase were blocked by strongly adsorbed carbon residues. Interestingly, the HDS reaction did not cause significant changes of the properties of the carbon-stabilized MoS_2. Conversely, the reference MoS_2 was strongly activated, in particular with respect to ethene hydrogenation, which can be explained by a pronounced sulfur loss during the HDS reaction, without significant site blockage by the coke deposited.

1. Introduction

Unsupported MoS_2-based catalysts have received considerable attention in industry and academia. They exhibit attractive activities in hydrorefining reactions, which has recently resulted in the development of a technical catalyst system by Exxon and Akzo (now Albermarle, cf. reviews [1–3]). Several synthesis methods for such catalysts are available, which were reviewed in [3,4]. Carbon-containing Mo sulfide catalysts [5–7] have attracted considerable attention owing to their interesting catalytic properties and their porosity. Recently, it was shown that promotion of unsupported MoS_2 with Ni can be achieved by thermal decomposition of thiosalt mixtures, e.g. tetrapropyl ammonium thiomolybdate (TPA-TM) with nickel diethenetriamine thiomolybdate. The effect of the Ni promoter differed significantly depending on the type of MoS_2 precursor employed – either TPA-TM, which is a typical precursor for the generation of carbon-stabilized porous MoS_2, or ammonium tetra thiomolybdate (ATM) [8]. The catalysts prepared with ATM were significantly less active, displayed lower values for the specific surface areas and showed a very different selectivity. Obviously, the precursor materials must behave different and the different properties of the catalysts in the HDS reaction call for further characterization effort.

In a first step, such characterization has been carried out for the unpromoted MoS_2 catalysts prepared from TPA-ATM and from ATM. The aim of the investigation was to establish a more detailed picture of the catalytic surfaces available. For this purpose, test reactions have been applied together with other characterization techniques [9–11]. It is well known that chemisorption methods alone do not reveal the distribution of coordinatively unsaturated Mo sites (Mo_{cus}) with different numbers of sulfur vacancies (^{3}M, ^{2}M, ^{1}M), which may play a key role for the catalytic activity. In this situation, test reactions such as ethene hydrogenation being specific for ^{3}M sites, cis–trans

* Corresponding authors. Laboratory of Industrial Chemistry, Ruhr University Bochum, P. O. Box 102148, D-44780 Bochum, Germany. Tel.: +49 234 322 2088; fax: +49 234 321 4115.
E-mail address: w.gruenert@techem.rub.de (W. Grünert).
[1] Present address: Leibniz Institute for Catalysis at Rostock University, Albert-Einstein-Strasse 29a, D-18059 Rostock, Germany.
[2] Present address: Universidad del Papaloapan, Circuito Central 200, Parque Industrial Tuxtepec 68301, Oaxaca, Mexico.
[3] Present address: Crenox Pigments GmbH, Rheinuferstraße 7-9, D-47829 Krefeld, Germany.

1566-7367/$ – see front matter © 2010 Elsevier B.V. All rights reserved.
doi:10.1016/j.catcom.2010.09.011

isomerization of 2-butene indicating ^{1}M sites, and H_2/D_2 scrambling, which may probably proceed both on ^{2}M and ^{3}M sites [10,11], may yield valuable complementary information.

This methodology comprising spectroscopic and catalytic tools was validated with a reference MoS_2 prepared via low-temperature ATM decomposition [9,10] and has been applied to a mechanochemically activated microcrystalline MoS_2 [11]. In the present study we examine its potential on materials of more practical interest. A carbon-stabilized mesoporous MoS_2 prepared by thermolysis of TPA-TM and the reference MoS_2 were investigated both before and after use in the hydrodesulfurization (HDS) of dibenzothiophene (DBT) (for results of the HDS study – see [8]) in order to document how changes caused in the two catalysts are reflected by our techniques.

2. Experimental

Mesoporous MoS_2 ("MoS_2(p)") was obtained by thermal decomposition of TPA-TM, which was inserted into a rotating furnace at 373 K and heated to 600 K in flowing nitrogen in 90 min. Subsequently, the product was cooled to 523 K and kept for 30 min before cooling to room temperature. The composition was determined (EURO Vector EA Combustion analyzer) to $MoS_{1.95}C_{0.80}H_{0.52}N_{0.06}$ A batch of this material was used in hydro-treatment experiments (autoclave, DBT dissolved in decaline, 3.4 MPa H_2, 623 K, duration 5 h, for details see [8]), after which a composition of $MoS_{1.60}C_{0.63}H_{1.25}N_{0.03}$ was found ("MoS_2(p/HDS)"). Details about the preparation of the reference MoS_2 by low-temperature ATM decomposition are given in [9]. The batch $MoS_2(A_1)$ used here will be further labeled MoS_2(ref). Its initial composition of $MoS_{2.4}$ changed to $MoS_{2.04-2.11}$ after the activation treatments applied [9] (see below). MoS_2 prepared from this batch was also studied after HDS of DBT (composition: $MoS_{1.59}C_{0.04}H_{1.4}$, "$MoS_2$(ref/HDS)"). In the characterization studies, comparison will be made with data of a microcrystalline, completely stoichiometric MoS_2, which was prepared by high-temperature ATM decomposition (for details see [9,11]).

X-ray powder patterns were recorded with a STOE STADI-P instrument (monochromatized $CuK_{\alpha 1}$ radiation, $\lambda = 1.54056$ Å). The apparent size of coherent scattering domains was calculated from the Scherrer equation using the (002) reflection. Most X-ray photoelectron spectra (Mo 3d, S 2p, O 1s, N 1s, and C 1s lines) were recorded with a Scienta/Specs/Prevac Surface analysis system (monochromatized Al anode, 14 kV*55 mA). For technical reasons, one sample was studied with a Leybold LH 10 spectrometer, upgraded with an EA 10/100 Specs multichannel detector (MgKα excitation, 10 kV*20 mA). Freshly synthesized or activated catalysts were handled under inert gas, including a transfer from the glove box to the spectrometer load lock by means of a sample transfer shuttle (Prevac, with in-house modifications, cf. [9]). Used samples were handled with air contact. EXAFS spectra at the Mo*K* edge (20000 eV) were measured in transmission mode at X1 station of Hasylab (Desy, Hamburg, Germany, see [9] for details). Freshly synthesized samples were pressed into suitable wafers in a glove box and sealed air-tight in kapton tape before exposing them to the X-ray beam. *N_2 physisorption* isotherms were measured with a Quantachrome Autosorb-1 MB instrument. Samples were evacuated at 523 K if not stated otherwise. Pore size distributions were derived from the desorption branches using the BJH formalism.

Transmission Electron Microscopy (TEM) investigations were performed with a Tecnai 30 STwin microscope (300 kV, FEG cathode, $C_S = 1.2$ mm). The samples for TEM investigations were prepared as follows. Small amount of powder containing mesoporous MoS_2 was suspended in methanol and ultrasonically grinded for 15 min. Afterwards, a transfer of the suspended powder on a TEM support (a lacey carbon film on 200 mesh cooper grid) was carried out by dipping of the TEM support into the solution. The prepared TEM samples were dried at a room temperature for several minutes. All images were recorded with a Gatan Multiscan CCD camera (2k×2k) and evaluated (including Fourier analyses) with a program Digital Micrograph (Gatan). EDS analyses were performed in the TEM mode with a Si/Li detector (EDAX System).

For catalysis and chemisorption studies, a setup characterized by facile switching options between batch (cycle) and flow regime and between pretreatment by thermoevacuation and reaction has been used (for details see [10]). It allowed performing pulse oxygen chemisorption (OCS) prior to catalysis (reactivation after OCS by treatment in 10% H_2/He at 473 K for 1 h). The catalysts (0.1 g per run) were investigated mostly after activation by reduction in H_2 (10% in He) for 3 h at 573 K, which will be designated as $\mathbf{R}_{573}$. Some experiments have been also performed after $\mathbf{R}_{573}$ preceded by a thermoevacuation (rotary pump) at 723 K for 4 h ($\mathbf{V}_{723}/\mathbf{R}_{573}$) or after mere thermoevacuation at 723 K ($\mathbf{V}_{723}$). After the activation, one of the following procedures was performed:

- OCS in pulse mode at 273 K, with mass-spectrometric detection (Pfeiffer QME 125),
- Determination of exchangeable surface hydrogen (H-Exc): after $\mathbf{R}_{573}$, samples were cooled to 473 K in 10% H_2/Ar which was then replaced by pure Ar keeping the temperature until the $m/e = 2$ QMS signal was constant. After cooling to room temperature, the reactor was reheated up to 573 K in a slow flow of D_2 (10% in Ar), and the quantity of HD evolved was determined by calibrated mass spectrometry.
- Catalysis was performed in recycle mode (for details see [10]). The reaction cycle was filled with the required reaction mixture, with the catalyst in a separate reactor loop under He. After heating the reactor to the desired temperature, the reactor loop was switched into the cycle, which resulted in the following initial concentrations: 2.4 vol.% ethene and 8 vol.% H_2 in He for ethene hydrogenation, 4 vol.% H_2 and 4 vol.% D_2 in He for H_2/D_2 scrambling. The reactions were followed with mass-spectrometric detection. Kinetic data for conversions up to 20% were used to evaluate first-order rate constants, including H_2/D_2 scrambling for which a first-order reaction kinetics has been reported earlier in the literature [12].

3. Results

3.1. Physicochemical characterization

The X-ray diffractograms of porous MoS_2(p), reference MoS_2(ref) and of a microcrystalline MoS_2 are compared in Fig. 1. Reflections of

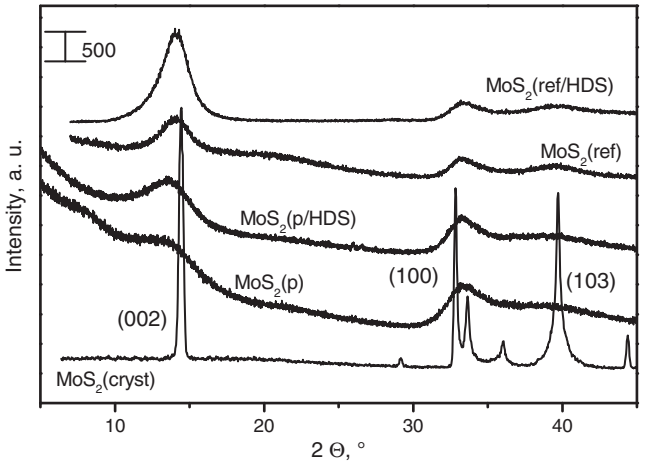

Fig. 1. X-ray diffractograms of MoS_2 materials investigated. The diffraction pattern of a microcrystalline MoS_2 made by high-temperature decomposition of ATM is given for comparison.

MoS_2(p) are significantly broader than those of MoS_2(ref), and the background intensity increases strongly towards smaller diffraction angles. The (002) reflection characterizing the stacking height of the MoS_2 layers gives an average particle size of 1.8 nm corresponding to just 3 layers. The average particle size of about 2.5 nm for MoS_2(ref) is somewhat larger, but did not change significantly during the HDS reaction. But for both samples a change of the intensity ratio (200)/(100)/(101)) is observed which is much more pronounced for MoS_2 (ref/HDS). We note that the (002) reflections of all disordered MoS_2 phases are shifted to lower diffraction angles relative to the microcrystalline MoS_2 sample suggesting that the lattice planes involved in this signal are bent, an observation reported for unsupported MoS_2 catalysts in [13,14]. For γ-Al_2O_3 supported Ni- and Co-MoS_2 catalysts one possible explanation for the curvature of MoS_2 layers was the incorporation of carbon in the MoS_2 structure [15]. On the other hand, the shift of the (002) reflection to lower scattering angles indicates an expansion of the *c*-axis which was reported for unsupported MoS_2 [14,16–18]. The expansion may be caused by strain effects, defects involved in folding or by the formation of H_xMoS_2 due to hydrogen intercalation in the van der Waals gaps [19]. The present materials MoS_2(p), MoS_2(p/HDS) and MoS_2(ref/HDS) all contain carbon and hydrogen (see above) and the bending of the layers is clearly seen in the HRTEM micrographs of MoS_2(p/HDS) (see below).

The EXAFS spectra of MoS_2(ref) and MoS_2(p) (Fig. 2) are very similar and in the Fourier-Transform (FT), no obvious difference in the first (Mo–S) shell can be seen whereas the second (Mo–Mo) shell is somewhat smaller for MoS_2(p). Model fits give slightly lower Mo–S and Mo–Mo coordination numbers for MoS_2(p) (Table 1), with differences being within the error limits. It has been reported that Mo carbide bonds are formed during exposure of MoS_2 to HDS conditions, and are characteristic for Mo sulfides prepared via thermolysis of alkylammonium thiosulfate as well [20–22]. With Co sulfide, simulations showed that replacement of S by C would diminish the first shell in the absolute value and affect the imaginary part of the FT spectra [23]. Our simulations with the FEFF code showed that with Mo, the influence on the imaginary part would be minor while the reduction of the absolute value would be prominent. Such influence was not observed with MoS_2(p) (Fig. 2), which indicates that the structural relation between Mo and C is geometrically ill defined. This suggests that carbon is not present as a carbide because Mo carbides possess well-ordered structures.

Table 1
Parameters of structural models obtained from the EXAFS spectra summarized in Fig. 1.

Sample	Shell	*r*, Å	C.N.	$10^3\ \sigma^2$, $Å^{-2}$
Microcrystalline MoS_2[a]	S	2.408 ± 0.003	5.2 ± 0.2	3.3 ± 0.3
	Mo	3.160 ± 0.002	6.6 ± 0.2	2.4 ± 0.1
MoS_2(ref)[a]	S	2.411 ± 0.002	5.3 ± 0.2	4.2 ± 0.3
	Mo	3.157 ± 0.002	3.6 ± 0.2	3.2 ± 0.2
MoS_2(p)	S	2.410 ± 0.005	5.1 ± 0.2	2.9 ± 0.2
	Mo	3.154 ± 0.006	3.3 ± 0.4	3.4 ± 0.2

[a] From Ref. [9].

The SAED pattern of the bright field image of MoS_2(p) after use in the HDS reaction (Fig. 3a) shows diffuse intensity on concentric rings. They can be indexed with the MoS_2-type structure. The slabs in Fig. 3b are short, bent and in the average form aggregates with 2–8 consecutive slabs. The nanoslabs are similar to those of MoS_2(ref) [11], but significantly shorter and of lower stacking number.

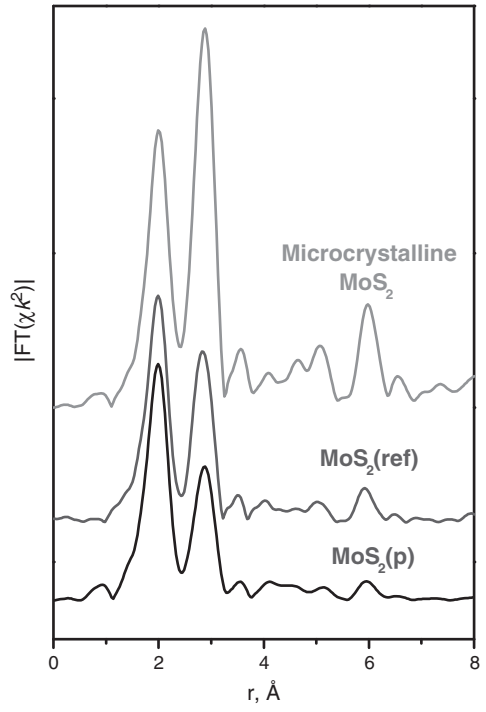

Fig. 2. MoK EXAFS spectra of mesoporous and reference MoS_2, compared with the spectrum of a microcrystalline MoS_2 made by high-temperature ATM decomposition. As-synthesized samples, stored in inert gas.

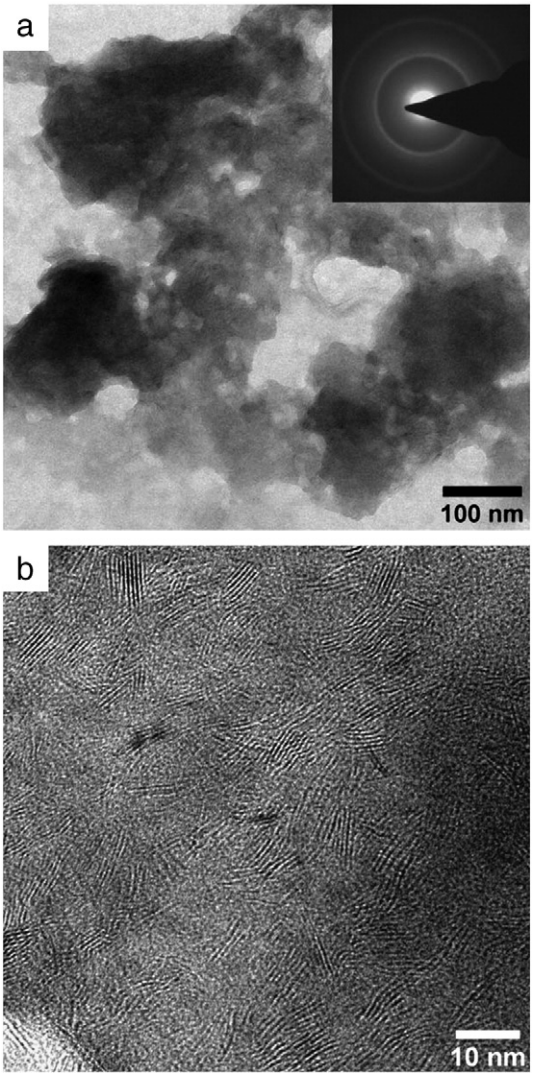

Fig. 3. (a) Bright-field TEM micrograph of MoS_2(p/HDS). The insert shows the SAED pattern. (b) high-resolution TEM micrograph recorded on an aggregation of nanoslabs.

X-ray photoelectron spectra of the samples are displayed in Fig. 4, in which survey spectra taken with monochromatized irradiation have been combined with a spectrum measured with a non-monochromatized source (MoS_2(ref/HDS)). As described in [9], the particular MoS_2 (ref) batch contained ammonium sulfate impurities [9] with typical binding energies for S and O of a SO_4^{2-} species and N1s located at a binding energy typical of NH_4^+ (Fig. 4c, d). The $\mathbf{R}_{573}$ treatment completely removed these impurities from the surface, the Mo lines appeared, S was now exclusively present as sulfide (Fig. 4a), and no N 1s and C 1s signals could be detected (not shown). The HDS reaction significantly altered the surface composition, and a thick carbon layer strongly interfered with the measurement of the remaining lines (Fig. 4b, MoS_2(ref/HDS)). Along with C 1s, the O 1s line was very intense and at a binding energy typical of sulfate (Fig. 4c). Indeed, in the S 2p region, a strong sulfate signal was seen together with the sulfide peak (Fig. 4a). In the Mo 3d region, a Mo(VI) state coexisted with Mo(IV), apparently, surface oxidation had affected not only the sulfide anions, but also Mo cations.

The surface of MoS_2(p) was clean already in the as-received state (see Fig. 4a), with a small O 1s signal located at a binding energy different from that of the SO_4^{2-} species (Fig. 4c). No C 1s emission below 284 eV indicative of carbide species could be discerned (Fig. 4b) A Mo $3d_{5/2}$ signal of Mo_2C expected at 227.8 eV [24] was not observed either (Fig, 4a), however, it would be detected between the strong Mo $3d_{5/2}$ and S 2s signals of the sulfide only at significant abundance of the carbide. The C 1s signal was of low intensity, suggesting that C is well distributed over the bulk. After catalysis, sulfate was again found (Fig. 4a, c, MoS_2(p/HDS)), but unlike the case of MoS_2(ref/HSD), the oxidation had not affected the Mo ions. Surprisingly, a N 1s line was found in the spectrum of MoS_2(p/HDS), which was *not* present before the HDS reaction (Fig. 4d). Whereas the sulfate species might well originate from air contact during catalyst handling after the catalytic experiment, this is highly unlikely in case of the nitrogen species. The feed used in the HDS runs did not contain nitrogen either. Apparently, nitrogen from the TPA-TM precursor, which was also detected by elemental analysis became exposed after activation and catalysis. Again, no signal that could be assigned to carbide species was detected in the C 1s region, where the signal intensity was low as opposed to the MoS_2 reference after HDS (Fig. 4b).

The porosity data of the catalysts studied are summarized in Fig. 5. It has been reported [9] that MoS_2(ref) develops a rather high BET surface area upon thermo-evacuation, with a pronounced abundance of pores around 4 nm size (Fig. 5a). MoS_2(p) has initially a higher BET surface area than MoS_2(ref), but upon outgassing at 723 K, it develops less porosity than the latter although its BET surface area increases as well. The samples differ most strongly in the porosity beyond 4 nm which is small in MoS_2(ref), whereas the distribution of MoS_2(p) extends far out towards the macropore region and includes significant contributions >20 nm (not shown). Conversely, the pore size distribution of MoS_2(ref) decays towards larger pore sizes (Fig. 5a). Upon thermoevacuation of MoS_2(p), smaller pores were strongly quenched when the most abundant 4 nm pores (Fig. 5b) were formed unlike in MoS_2(ref) where the 4 nm pores appear to be additional and their formation caused little perturbation of the remaining pore system (Fig. 5a). The HDS reaction had a different impact on the porosity of the two MoS_2 samples, causing a loss for MoS_2(p), but an increase for MoS_2(ref). The latter increase is reminiscent of the gain in BET surface area by thermoevacuation, which is due to loss of excess sulfur [9]. In MoS_2(p/HDS), the porosity was affected over the whole pore size range (Fig. 5b). Whereas the most abundant 4 nm pores appeared in this state as well, though less intense than after thermoevacuation, the smaller pores were completely quenched and the abundance of the larger pores was smaller than in the as-synthesized state.

The OCS capacities of the different samples are compared in Table 2. The tendency to expose Mo ions is much smaller in the carbon-containing materials (including the reference MoS_2 after HDS) than in the fresh MoS_2(ref). Among the 3 different MoS_2 batches studied in [9], the highest OCS capacity measured (obtained after $\mathbf{R}_{573}$

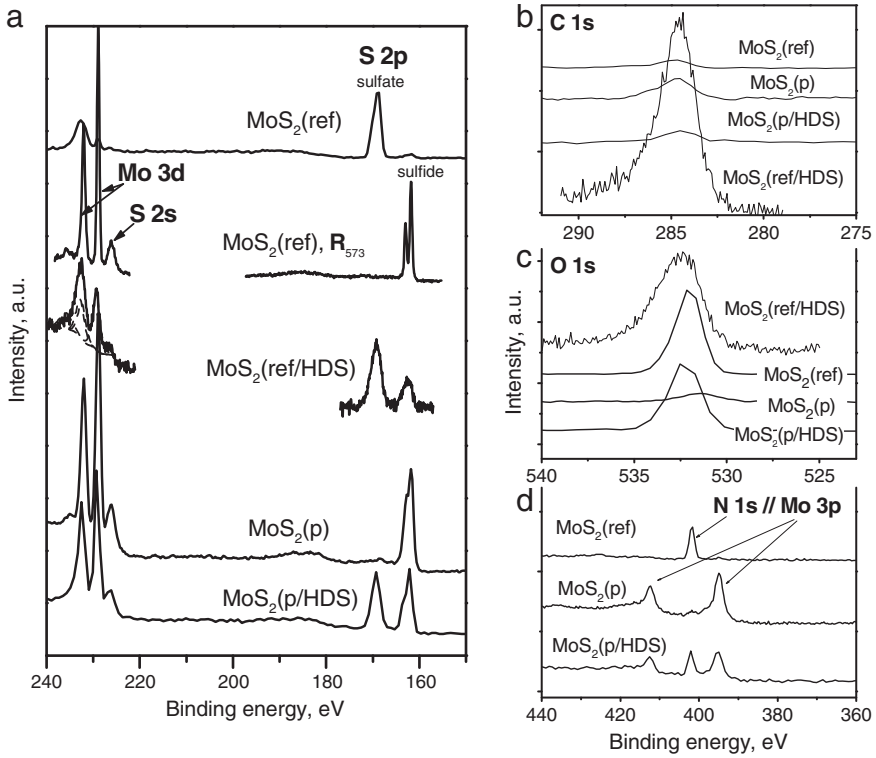

Fig. 4. X-ray photoelectron spectra of MoS_2 materials. a) Mo 3d/S 2p region, b) C 1s region, c) O 1s region, d) N 1s/Mo 3p region. As-synthesized samples, stored under inert gas, or catalysts after HDS, stored without precautions. MoS_2(ref), $\mathbf{R}_{573}$ was transferred from the reactor to the spectrometer via a glove box, cf. [9].

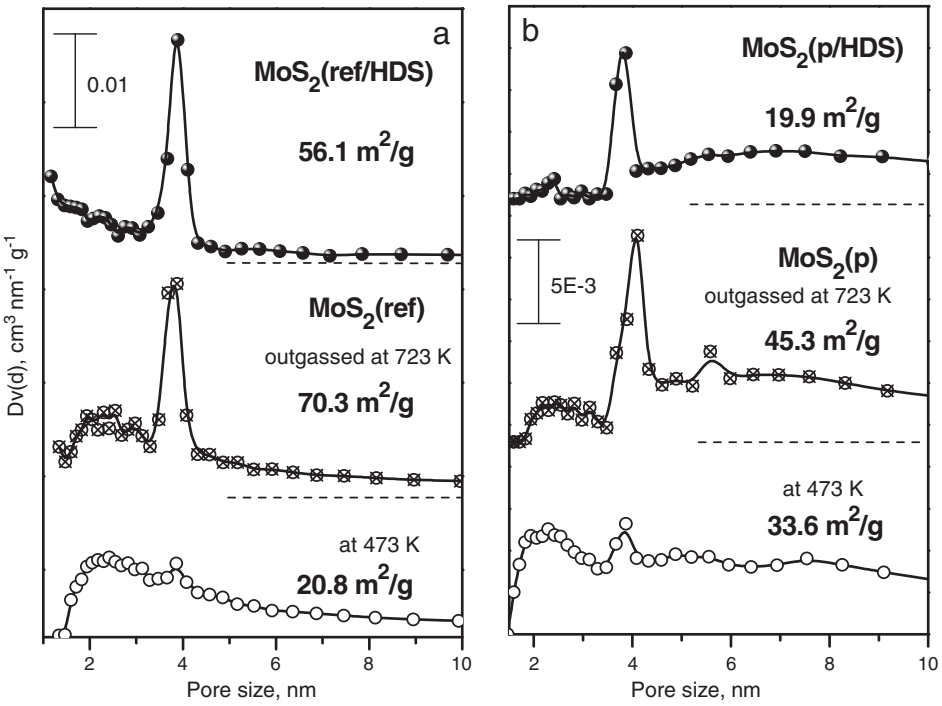

Fig. 5. Pore-size distributions (BJH method) of MoS_2 materials. a) materials derived from MoS_2(ref), b) materials derived from MoS_2(p). The BET surface areas obtained are given for comparison.

or $\mathbf{R}_{473}$) ranged between 34 and 60 μmol/g, whereas 11.3 μmol/g was the highest amount achieved with the carbon-containing samples studied here. However, with MoS_2(p), the ranking of the activation treatments with regard to vacancy formation ($\mathbf{V}_{723}/\mathbf{R}_{573}<\mathbf{R}_{573}$) was still the same as with MoS_2(ref) whereas it was reversed in MoS_2(ref/HDS). After use in HDS, thermoevacuation was not sufficient to create any vacancy at Mo at all.

Remarkable differences between MoS_2(ref) and MoS_2(p) are observed for the content of exchangeable hydrogen (Table 2). Whereas >100 μmol of exchangeable H [9] were detected per g MoS_2(ref) [9], the surface of MoS_2(p) was almost void of these species. After catalysis, the concentration of exchangeable hydrogen increased significantly on the latter catalyst, whereas it decreased on the reference MoS_2.

3.2. Catalysis

Catalytic studies with MoS_2 catalysts are always affected by deactivation phenomena, the extent of which was much larger with the carbon-containing MoS_2 materials than with MoS_2(ref). For ethene hydrogenation, conditions under which the reaction rate remained stable or could be restored by standard procedures used in [10] or even by repeating the $\mathbf{R}_{573}$ activation could not be established. In H_2/D_2 scrambling, stable activities were obtained over MoS_2(p) while minor, but significant deactivation occurred with MoS_2(p/HDS), in particular between the first and second run. This is quite surprising because the reaction does not produce deposits. Due to these stability problems, activity measurements have been performed for only one activation ($\mathbf{R}_{573}$) at individual temperatures, which may be different for different catalysts, whereas cis–trans isomerization of 2-butene, which is thought to be a test reaction for ^{1}M sites [10], was omitted. Comparison will be made with the properties of MoS_2(ref), for which catalytic data are available for the whole temperature range [10].

Kinetic data for ethene hydrogenation (Table 3) show rate constants being much smaller for MoS_2(p) before and after HDS than for MoS_2(ref). However, if related to the OCS capacity, this "rate per vacancy" (r_0/OCS) is almost identical for MoS_2(p) and MoS_2(ref). Whereas use in HDS causes only a slight activation of MoS_2(p) for hydrogenation, the impact on MoS_2(ref) was very drastic: the hydrogenation rate constant increased more than twentyfold, the rate per vacancy (r_0/OCS) by two orders of magnitude. This rate per vacancy is comparable with that of the most active state achieved earlier with MoS_2(ref) [10] (Table 3, footnote b).

The data for H_2/D_2 scrambling are collected in Table 4. Again, the absolute rates were lower for MoS_2(p) than for MoS_2(ref), but r_0/OCS is of the same order of magnitude. It has been described in [10] that the kinetic data for H_2/D_2 scrambling measured with MoS_2(ref) were

Table 2
Oxygen chemisorption capacities (OCS) and concentration of exchangeable surface hydrogen (H_{exc}).

Material	Pretreatment	OCS, μmol O_2/g		H_{exc}, μmol HD/g	
		Before[a]	After[b]	Before[a]	After[b]
		Catalysis		Catalysis	
MoS_2(ref)	$\mathbf{V}_{723}$	6.5	0	1	n. d.
	$\mathbf{R}_{573}$	60	7.6	109	39.5
	$\mathbf{V}_{723}/\mathbf{R}_{573}$	28	10.7	115	n. d.
MoS_2(p)	$\mathbf{V}_{723}$	3.4	0	n. d.	n. d.
	$\mathbf{R}_{573}$	9.8	11.3	5	24
	$\mathbf{V}_{723}/\mathbf{R}_{573}$	7.3	7.5	n. d.	n. d.

[a] MoS_2(ref) (data from Ref. [9]) and MoS_2(p).
[b] MoS_2(ref/HDS) and MoS_2(p/HDS).

Table 3
Ethlyene hydrogenation over different types of MoS_2 after $\mathbf{R}_{573}$ activation. Data from MoS_2(ref), taken from Ref. [10], Fig. 2 (Arrhenius curve), are given in brackets for comparison.

Material	T, K	10^4 k, l g^{-1} s^{-1}	$10^2 r_0$/OCS, s^{-1}
MoS_2(p)	463	1.0 [7.6]	1.0 [1.2]
MoS_2(p/HDS)	473	2.6 [9.4]	2.2 [1.5]
MoS_2(ref/HDS)	451	145 [6.0[a]]	190 [1.0[a]]

[a] For comparison: MoS_2(ref) after $\mathbf{R}_{573}/\mathbf{V}_{723}$ – $k = 7.6 * 10^{-2}$ l g^{-1} s^{-1}, r_0/OCS = 2.6 s^{-1}, extrapolated from Fig. 2, Ref. [10], Fig. 2.

Table 4
H_2/D_2 scrambling over different types of MoS_2 at 473 K after $\mathbf{R}_{573}$ activation. Data from MoS_2(ref), taken from Ref. [10], Fig. 2 (Arrhenius curve), are given in brackets for comparison.

Material	10^3 k, l g^{-1} s^{-1}	r_0/OCS, s^{-1}
MoS_2(p)	8.0[a] [18.3[a]]	1.5[a] [0.55[a]]
MoS_2(p/HDS)	1.4[b] [18.3[a]]	0.2[b] [0.55[a]]
MoS_2(ref/HDS)	(100) [18.3[a]]	(24) [0.55[a]]

[a] Influenced by transport limitation to different extents, see text.
[b] Second run (stable activity).

significantly affected by mass-transfer limitations: whereas the activation energy was ca. 17 kJ/mol under the standard conditions applied here, a value of ca. 65 kJ/mol was found below 373 K. Such data cannot normally be used for comparison of reaction rates because a separation of mass transfer and intrinsic kinetics would require involved measurements. It is, however, safe to conclude that the measured rate is lower than the intrinsic rate would be without the transport limitation, and this is the way the data will be employed here. The apparent rate constants measured with MoS_2(p) and with MoS_2(p/HDS) were significantly lower than those of MoS_2(ref), for the latter even by an order of magnitude (Table 4). Therefore, any mass-transfer influence should be smaller in these data, in case of MoS_2(p/HDS) probably absent. Therefore, among the r_0/OCS reported in Table 4, the value for MoS_2(p/HDS) (0.2 s^{-1}) is probably correct, that for MoS_2(ref) (0.55 s^{-1}) is definitely underestimated (*vide supra*), probably also that for MoS_2(p) (1.5 s^{-1}), but to a smaller extent. Hence, a clear activity difference can be stated in particular between MoS_2(p) and MoS_2(p/HDS), i.e., the use in HDS catalysis caused a loss in activity. Instead, the intrinsic r_0/OCS of MoS_2(p) and MoS_2(ref) might be rather similar as in the case of ethene hydrogenation, although this conclusion should be drawn with caution.

As opposed to MoS_2(p), MoS_2(ref) was significantly activated by the use in HDS catalysis also for H_2/D_2 exchange (Table 4). The extent of activation seems to be smaller than in case of hydrogenation (Table 3), but again, the H_2/D_2 data have to be taken with caution as mass-transfer effects could not yet be completely suppressed in the measurements with MoS_2(ref/HDS), which gave an apparent activation energy of ≈38 kJ/mol.

4. Discussion

Strong differences between MoS_2 samples prepared via different routes and between fresh catalysts and samples used in a HDS reaction were observed. Some results are quite surprising but give deeper insights in particular structural features of the materials.

MoS_2 prepared by thermolysis of ATM and the "porous", carbon containing material derived from TPA-TM exhibit a similar size of the accessible surface area, but a very different pore-size distribution (Fig. 5), which is very broad for MoS_2(p). Slit pores of 4 nm diameter evolved upon thermoevacuation for both samples (cf. [9] for MoS_2 (ref)), an effect observed also for a microcrystalline MoS_2 activated by ball milling [10,11]. This is quite surprising: whereas these pores were obviously formed at the expense of excess sulfur in MoS_2(ref), with a concomitant decrease of the S/Mo ratio from 2.4 to 2.1, both MoS_2(p) and the ball-milled microcrystalline MoS_2 are sulfur deficient (S/Mo = 1.95 and 1.60, respectively). It seems, therefore, that this structural motif may be of particular stability. In MoS_2(p) it was apparently formed by breakdown of smaller pores.

In the X-ray powder patterns (Fig. 2), the major reflections of 2H-MoS_2 are observed for all samples but being broader than in MoS_2(ref) indicative for a lower stacking number of MoS_2. HRTEM micrographs of MoS_2(ref/HDS) (Fig. 3) support this assumption. On this basis one might have expected larger differences also in the EXAFS spectra of MoS_2(ref) and MoS_2(p) (Fig. 3, Table 1), where the Mo–Mo shell is indicative of the slab diameter. It has been suggested that EXAFS underestimates the size of MoS_2 platelets due to a displacement of Mo atoms in the external row of the MoS_2 platelets [25]. This model is, however, based on the assumption of flat slabs, which may well fail for present materials characterized by bent slabs. Thus, there is certainly a need for a more detailed XAFS study of such materials.

Despite the less ordered structure and the significant sulfur deficit, MoS_2(p) did not exhibit any tendency for an increased vacancy formation or catalytic activity. Instead, the OCS capacity after $\mathbf{R}_{573}$ or $\mathbf{V}_{723}/\mathbf{R}_{573}$ was 1/6 to 1/4 of those found for MoS_2(ref), and the rates per vacancy for ethene hydrogenation and H_2/D_2 scrambling (after $\mathbf{R}_{573}$) resembled those of MoS_2(ref) (Tables 3 and 4). This is surprising because a decrease of sulfur content should favor the hydrogenation reaction, and also H_2/D_2 scrambling, as observed for MoS_2(ref) [10,11] and also for the ball-milled microcrystalline MoS_2 [10,11]. Indeed, this case can be observed in the present study as well, because the sulfur deficient MoS_2(ref/HDS) sample (S/Mo = 1.6) is highly active for both test reactions. MoS_2(p) behaves completely different and a reasonable explanation may be that the S deficiency is largely saturated by adsorbed hydrocarbon residues intrinsically formed during decomposition of the precursor which could not easily be removed in the reductive activation treatments performed.

Use in the HDS reaction caused significant structural changes, which were very different for MoS_2(ref) and MoS_2(p). The results suggest that not only some C residues are deposited on the surfaces but also thorough rearrangements of the structure occur during HDS. The rather high hydrogen content may be related to the C present in MoS_2(p/HDS), but such explanation is not possible for MoS_2(ref/HDS) containing only minute amounts of carbon. Because HDS is performed at high H_2 pressure, the two samples may contain bulk hydrogen being absorbed under these conditions [26].

There is not much difference between the X-ray diffractograms of MoS_2(p) and MoS_2(p/HDS) (Fig. 1). However, the observation of a significant N 1s signal in the XP spectrum of MoS_2(p/HDS) (Fig. 4d) and the strong changes in the pore-size distribution (Fig. 5b) suggest that species initially located in the bulk moved to (or near to) the external surface and that the pore structure was rearranged. Surprisingly, the composition of MoS_2(p) was hardly modified by use in HDS, the C/Mo ratio remained in the range 0.6 ... 0.8. This was confirmed by XPS: while the C 1s peak appears to be lower in MoS_2(p/HDS) (Fig. 4b), the C 1s/Mo 3d intensity ratio remained indeed unchanged, the difference being rather due to a sulfate overlayer created by surface oxidation. Hence the considerable changes in the pore size distribution are due to morphological reconstructions and not to pore plugging by carbonaceous residues.

For MoS_2(p/HDS) and MoS_2(ref/HDS), mere thermoevacuation could not create Mo_{cus} that might be detected by OCS. This may be due to the initially rather significant surface oxidation (Fig. 4a, c) or to site blockage by carbonaceous species. It has been shown in [9] that $\mathbf{V}_{723}$ effectively removes all sulfate from the surface, and MoS_2(ref), which was initially contaminated by sulfate as well, did adsorb oxygen after $\mathbf{V}_{723}$ (Table 2). Hence, carbonaceous species blocking the Mo_{cus} sites present on the surfaces of MoS_2(p/HDS) and MoS_2(ref/HDS) appear to withstand thermoevacuation. After $\mathbf{R}_{573}$, the OCS capacity of MoS_2(p/HDS) was somewhat higher than that of MoS_2(p) but the change of properties after HDS catalysis is better documented by the significantly increased H_2/D_2 exchange capacity of MoS_2(p), which may be a result of the exposure to high H_2 pressures. Still, the amount of exchangeable hydrogen was low in both MoS_2(p/HDS) and MoS_2(ref/HDS). This is in strong contrast to the large total H content, supporting the assumption that much of the hydrogen was absorbed in the bulk.

The catalytic properties of MoS_2(p/HDS)) and MoS_2(p) are similar. Whereas hydrogenation was somewhat accelerated as compared to MoS_2(ref) (in terms of r_0/OCS, cf. Table 3), H_2/D_2 exchange was slightly attenuated (cf. Table 4). This alludes the trend expected for a strongly sulfur deficient surface, the attenuation of H_2/D_2 scrambling probably being due to a net loss of ^{2}M sites in favor of (inactive) ^{4}M

sites [11]. In MoS_2(ref), the changes caused by its use in HDS (e.g. loss of sulfur) were more clearly reflected in the catalytic properties. Both ethene hydrogenation and H_2/D_2 scrambling were accelerated, as expected due to the sulfur deficit. This emphasizes once more the different role of the C species present in MoS_2(p) (before and after catalysis) and in MoS_2(ref/HDS). In the latter, the carbon was predominantly at the external surface (see XPS results, Fig. 4), apparently blocking active sites (no OCS capacity after $\mathbf{V}_{723}$, Table 2). But those sites uncovered after $\mathbf{R}_{573}$ were highly unsaturated and provided good activity in hydrogenation, and also in H_2/D_2 scrambling. In contrast, C species in MoS_2(p) are part of the structure being well distributed over the bulk of the sample, and even at the surfaces C was only removed to a minor extent by $\mathbf{R}_{573}$. The catalytic activity typical for a near-stoichiometric MoS_2 apparently was provided by the near-stoichiometric MoS_2 nanoslabs.

An important result of our study is that neither XPS nor EXAFS gave any hints for the presence of carbidic species. Careful inspection of Figs. 2 and 4 let us conclude that no carbide was present in MoS_2(p). According to reports in literature [21,22] HDS should result in carbidization of the MoS_2 edges, but such species were not detected in the C 1s or Mo 3d spectra either. MoS_2(p/HDS) and MoS_2(ref/HDS) were stored in air after HDS test and two scenarios can be envisaged. Surface carbide species may have been oxidized to surface carbonates or gaseous carbon oxides. Because carbonate was not observed in XPS, desorption of carbon oxides would have left bare Mo sites at the surface which are then oxidized readily. But no such Mo oxide species were found in the surface region of MoS_2(p/HDS), therefore we prefer the view that Mo carbide species were not formed during catalysis at least on this material.

It remains to be discussed how much these methods are appropriate to predict or reflect the catalytic data shown by these materials in the HDS of DBT. It can be seen in [8] that despite significant differences in the promoted catalysts, the reaction rates obtained with unpromoted MoS_2(ref) and MoS_2(p) were rather similar, with a slightly higher contribution of the hydrogenation path (relative to the direct desulfurization path) over MoS_2(p). This is apparently incongruent with the results obtained in our study where MoS_2(ref/HDS) was the catalyst with the higher (ethene) hydrogenation activity. Therefore, a reaction that could mimic C–S bond cleavage as well as an aromatic hydrogenation should be probably included into the set of test reactions. However, the results reported here show that already the present approach combining spectroscopic, adsorption and simple catalytic tools yields a very detailed picture of structural properties of the different MoS_2 samples.

5. Conclusions

Structural and surface properties of mesoporous, carbon-containing MoS_2 prepared by thermolysis of TPA-ATM and of a reference MoS_2 obtained by thermal decomposition of ATM were investigated before and after use of these catalysts in the HDS of DBT. A characteristic feature of the carbon-stabilized MoS_2 was a broad pore-size distribution tailing into the macropore region, and a heterogeneous structure with nanoslabs of $\approx$2 nm stacking height embedded in an amorphous matrix. During thermal treatment, mesopores of $\approx$4 nm size were formed in the mesoporous MoS_2 similar as in the reference MoS_2 although their initial S content was quite different. In the reference MoS_2, these pores were formed by removal of excess sulfur, whereas in the sulfur-deficient carbon-stabilized MoS_2 mesopores were formed by breakdown of micropores. The key message of XPS and EXAFS investigations is the failure to detect carbide species despite the well distributed carbon in MoS_2(p).

After thermal activation treatments, the exposure of Mo sites (measured by OCS) was smaller for MoS_2(p) than for MoS_2(ref), but their activity patterns (related to the OCS capacity) were similar. This result suggests that S vacancies of MoS_2(p) were blocked by strongly adsorbed carbon residues while the catalytic properties are supported by a nearly stoichiometric phase, apparently the MoS_2 nanoslabs. After use in HDS, the properties of MoS_2(p) were similar as before despite the change of the chemical composition, and only microporosity was destroyed. In contrast, the catalytic activity of the reference MoS_2 was significantly enhanced. This can be explained by the significant loss of sulfur favoring, in particular, the hydrogenation reaction, without interference by a considerable amount of surface carbon detected in a post-catalytic XPS measurement.

Acknowledgements

Financial support by the German Science foundation is gratefully acknowledged (grants No. Gr 1447-15 and Be-1653/11). We thank Dr. Monica Guraya for XPS measurements, Dr. Zhida Huang for XRD analyses and Ms. Susanne Buse for the physisorption measurements.

References

[1] T.C. Ho, Catal. Today 98 (2004) 3.
[2] T.C. Ho, Catal. Today 130 (2008) 206.
[3] S. Eijsbouts, S.W. Mayo, K. Fujita, Appl. Catal. A 322 (2007) 58.
[4] M. Breysse, C. Geantet, P. Afanasiev, J. Blanchard, M. Vrinat, Catal. Today 130 (2008) 3.
[5] G. Alonso, G. Berhault, A. Aguilar, V. Collins, C. Ornelas, S. Fuentes, R.R. Chianelli, J. Catal. 108 (2002) 359.
[6] G. Alonso, G. Berhault, F. Paraguay, E. Rivera, S. Fuentes, R.R. Chianelli, Mater. Res. Bull. 38 (2003) 1045.
[7] G. Alonso, M. DelValle, J. Cruz, V. Petranovskii, A. Licea-Claverie, S. Fuentes, Catal. Lett. 43 (1998) 117.
[8] M. Poisot, W. Bensch, S. Fuentes, C. Ornelas, G. Alonso, Catal. Lett. 117 (2007) 43.
[9] M. Polyakov, M.W.E. van den Berg, T. Hanft, M. Poisot, W. Bensch, M. Muhler, W. Grünert, J. Catal. 256 (2008) 126.
[10] M. Polyakov, M. Poisot, W. Bensch, M. Muhler, W. Grünert, J. Catal. 256 (2008) 137.
[11] M. Polyakov, S. Indris, S. Schwamborn, A. Mazhejka, M. Poisot, L. Kienle, W. Bensch, M. Muhler, W. Grünert, J. Catal. 260 (2008) 236.
[12] R.L. Wilson, C. Kemball, A.K. Galwey, Trans. Faraday Soc. 58 (1962) 583.
[13] Y. Iwata, Y. Miki, K. Sato, T. Yoneda, Y. Sugimoto, A. Nishijima, H. Shimada, Catal. Today 45 (1998) 353.
[14] M.M. Mdleleni, T. Hyeon, K.S. Suslick, J. Am. Chem. Soc. 120 (1998) 6189.
[15] S. Eijsbouts, L.C.A. van den Oetelaar, R.R. van Puijenbroek, J. Catal. 229 (2005) 352.
[16] K.S. Liang, R.R. Chianelli, F.Z. Chien, S.C. Moss, J. Non-Cryst. Solids 79 (1986) 251.
[17] M. Chhowalla, G.A.J. Amaratunga, Nature 407 (2000) 164.
[18] C.J. Wright, C. Sampson, D. Fraser, R.B. Moyes, P.B. Wells, C. Riekel, J. Chem, Soc, Faraday Trans. I 76 (1980) 1585.
[19] Y. Feldman, E. Wasserman, D.J. Srolovitz, T. Tenne, Science 267 (1995) 222.
[20] R.R. Chianelli, G. Berhault, Catal. Today 53 (1999) 357.
[21] G. Berhault, A. Mehta, A.C. Pavel, J.Z. Yang, J.Z. Rendon, M.J. Yacaman, L.C. Araiza, A.D. Moller, R.R. Chianelli, J. Catal. 198 (2001) 9.
[22] S.P. Kelty, G. Berhault, R.R. Chianelli, Appl. Catal. A 322 (2007) 9.
[23] C. Glasson, C. Geantet, M. Lacroix, F. Labruyere, P. Dufresne, J. Catal. 212 (2002) 76.
[24] C.D. Wagner, A.V. Naumkin, A. Raut-Vass, J.W. Allison, C.J. Powell, J.R. Rumble Jr., NIST X-ray Photoelectron Spectroscopy Database, National Institute of Standards and Technology, 2003.
[25] T. Shido, R. Prins, J. Phys. Chem. B 102 (1998) 8426.
[26] P.N. Jones, E. Knözinger, W. Langel, R.B. Moyes, J. Tomkinson, Surf. Sci. 207 (1989) 159.